Broadband light absorption enhancement in polymer photovoltaics using metal nanowall gratings as transparent electrodes

Zhuo Ye,[1,2,*] Sumit Chaudhary,[3] Ping Kuang,[1,4] and Kai-Ming Ho[1,2,5]

[1]*Ames Laboratory - USDOE, Ames, Iowa 50011, USA*
[2]*Department of Physics and Astronomy, Iowa State University, Ames, Iowa 50011 USA*
[3]*Department of Electrical and Computer Engineering, Iowa State University, Ames, Iowa 50011, USA*
[4]*Department of Materials Science and Engineering, Iowa State University, Ames, Iowa 50011 USA*
[5]*kmh@ameslab.gov*
[*]*zye@iastate.edu*

Abstract: The authors investigate light absorption in organic solar cells in which indium tin oxide (ITO) is replaced by a new metallic architecture (grating) as a transparent electrode. Different from typical metal nanowire gratings, our gratings consist of metal nanowalls with nanoscale footprint and (sub)microscale height [Adv. Mater. **23**, 2469 (2011)], thus ensuring high optical transmittance and electrical conductivity. Simulations reveal that a broadband and polarization-insensitive light absorption enhancement is achieved via two mechanisms, when such silver nanowall gratings are employed in P3HT:PCBM based solar cells. Overall absorption enhanced by ~23% compared to a reference cell with ITO electrode.

OCIS codes: (350.6050) Solar energy; (350.2770) Gratings; (160.4890) Organic materials.

References and links

1. M. W. Rowell, M. A. Topinka, M. D. McGehee, H. J. Prall, G. Dennler, N. S. Sariciftci, L. Hu, and G. Gruner, "Organic solar cells with carbon nanotube network electrodes," Appl. Phys. Lett. **88**(23), 233506 (2006).
2. B. O'Connor, C. Haughn, K.-H. An, K. P. Pipe, and M. Shtein, "Transparent and conductive electrodes based on unpatterned, thin metal films," Appl. Phys. Lett. **93**(22), 223304 (2008).
3. J. B. Wu, H. A. Becerril, Z. Bao, Z. Liu, Y. Chen, and P. Peumans, "Organic solar cells with solution-processed graphene transparent electrodes," Appl. Phys. Lett. **92**(26), 263302 (2008).
4. P. Kuang, J.-M. Park, W. Leung, R. C. Mahadevapuram, K. S. Nalwa, T.-G. Kim, S. Chaudhary, K.-M. Ho, and K. Constant, "A new architecture for transparent electrodes: relieving the trade-off between electrical conductivity and optical transmittance," Adv. Mater. (Deerfield Beach Fla.) **23**(21), 2469–2473 (2011).
5. G. Yu, J. Gao, J. C. Hummelen, F. Wudl, and A. J. Heeger, "Polymer photovoltaic cells: Enhanced efficiencies via a network of internal donor-acceptor heterojunctions," Science **270**(5243), 1789–1791 (1995).
6. C. J. Brabec, N. S. Sariciftci, and J. C. Hummelen, "Plastic solar cells," Adv. Funct. Mater. **11**(1), 15–26 (2001).
7. Y. Kim, S. Cook, S. M. Tuladhar, S. A. Choulis, J. Nelson, J. R. Durrant, D. D. C. Bradley, M. Giles, I. Mcculloch, C.-S. Ha, and M. Ree, "A strong regioregularity effect in self-organizing conjugated polymer films and high-efficiency polythiophene:fullerene solar cells," Nat. Mater. **5**(3), 197–203 (2006).
8. J. A. Hauch, P. Schilinsky, S. A. Choulis, R. Childers, M. Biele, and C. J. Brabec, "Flexible organic P3HT:PCBM bulk-heterojunction modules with more than 1 year outdoor lifetime," Sol. Energy Mater. Sol. Cells **92**(7), 727–731 (2008).
9. G. Li, V. Shrotriya, J. Huang, Y. Yao, T. Moriarty, K. Emery, and Y. Yang, "High-efficiency solution processable polymer photovoltaic cells by self-organization of polymer blends," Nat. Mater. **4**(11), 864–868 (2005).
10. M. Reyes-Reyes, K. Kim, and D. L. Carroll, "High-efficiency photovoltaic devices based on annealed poly(3-hexylthiophene) and 1-(3-methoxycarbonyl)-propyl-1-phenyl-(6,6)C61 blends," Appl. Phys. Lett. **87**(8), 083506 (2005).
11. T. Kirchartz, K. Taretto, and U. Rau, "Efficiency limits of organic bulk heterojunction solar cells," J. Phys. Chem. C **113**(41), 17958–17966 (2009).
12. T. H. Reilly III, J. Lagemaat, R. C. Tenent, A. J. Morfa, and K. L. Rowlen, "Surface-plasmon enhanced transparent electrodes in organic photovoltaics," Appl. Phys. Lett. **92**(24), 243304 (2008).
13. F.-C. Chen, J.-L. Wu, C.-L. Lee, Y. Hong, C.-H. Kuo, and M. H. Huang, "Plasmonic-enhanced polymer photovoltaic devices incorporating solution-processable metal nanoparticle," Appl. Phys. Lett. **95**(1), 013305 (2009).

#161810 - $15.00 USD Received 19 Jan 2012; revised 21 Mar 2012; accepted 28 Mar 2012; published 15 May 2012

14. S. Pillai, K. R. Catchpole, T. Trupke, and M. A. Green, "Surface Plasmon enhanced silicon solar cells," J. Appl. Phys. **101**(9), 093105 (2007).
15. H. Shen, P. Bienstman, and B. Maes, "Plasmonic absorption enhancement in organic solar cells with thin active layers," J. Appl. Phys. **106**(7), 073109 (2009).
16. B. P. Rand, P. Peumans, and S. R. Forrest, "Long-range absorption enhancement in organic tandem thin-film solar cells containing silver nanoclusters," J. Appl. Phys. **96**(12), 7519–7526 (2004).
17. N. C. Lindquist, W. A. Luhman, S. H. Oh, and R. J. Holmes, "Plasmonic nanocavity arrays for enhanced efficiency in organic photovoltaic cells," Appl. Phys. Lett. **93**(12), 123308 (2008).
18. M. A. Sefunc, A. K. Okyay, and H. V. Demir, "Plasmonic backcontact grating for P3HT:PCBM organic solar cells enabling strong optical absorption increased in all polarizations," Opt. Express **19**(15), 14200–14209 (2011).
19. K. S. Nalwa, J. M. Park, K. M. Ho, and S. Chaudhary, "On realizing higher efficiency polymer solar cells using a textured substrate platform," Adv. Mater. (Deerfield Beach Fla.) **23**(1), 112–116 (2011).
20. Z. Y. Li and L. L. Lin, "Photonic band structures solved by a plane-wave-based transfer-matrix method," Phys. Rev. E Stat. Nonlin. Soft Matter Phys. **67**(4), 046607 (2003).
21. Z. Ye, X. Hu, M. Li, K. M. Ho, and P. Yang, "Propagation of guided modes in curved nanoribbon waveguides," Appl. Phys. Lett. **89**(24), 241108 (2006).
22. ISU TMM simulation package (2010). *http://www.public.iastate.edu/~mli/homepage.html*.
23. M. G. Kang, T. Xu, H. J. Park, X. Luo, and L. J. Guo, "Efficiency enhancement of organic solar cells using transparent plasmonic Ag nanowire electrodes," Adv. Mater. (Deerfield Beach Fla.) **22**(39), 4378–4383 (2010).
24. E. D. Palik, *Handbook of Optical Constants of Solids* (Academic Press: Orlando FL, 1985).
25. Database, "Optical constants of In_2O_3-SnO_2 (ITO, Indium tin oxide)." *http://refractiveindex.info/?group=CRYSTALS&material=ITO*.
26. A. J. Moulé and K. Meerholz, "Interference method for the determination of the complex refractive index of thin polymer layers," Appl. Phys. Lett. **91**(6), 061901 (2007).
27. A. W. Hains, J. Liu, A. B. F. Martinson, M. D. Irwin, and T. J. Marks, "Anode interfacial tuning via electron-blocking/hole-transport layers and indium tin oxide surface treatment in bulk-heterojunction organic photovoltaic cells," Adv. Funct. Mater. **20**(4), 595–606 (2010).
28. M. R. Lee, R. D. Eckert, K. Forberich, G. Dennler, C. J. Brabec, and R. A. Gaudiana, "Solar power wires based on organic photovoltaic materials," Science **324**(5924), 232–235 (2009).
29. L. A. A. Pettersson, S. Ghosh, and O. Inganäs, "Optical anisotropy in thin films of poly(3,4-ethylenedioxythiophene)–poly(4-styrenesulfonate)," Org. Electron. **3**(3-4), 143–148 (2002).

1. Introduction

Indium tin oxide (ITO) is one of the most widely used transparent electrodes for solar cells and light-emitting devices because of its electrical conductivity as well as optical transparency. However, due to limited supply of indium, high cost, and the brittle nature of ITO, alternatives are being sought and evaluated, including carbon nanotube networks, thin metal films, and graphene films [1–3]. In a recent work [4], we proposed a new architecture for transparent electrodes, which consists of high aspect-ratio metal nanowall gratings held by a polymer matrix. Experimental measurements showed that such structures have excellent optical and electrical properties, and thus a promising replacement for ITO. Bulk heterojunction organic photovoltaic (OPV) cells, have been receiving increasing attention in the recent years because of their great potential for cost-effective solar energy harvesting devices [5–8]. The most commonly used materials for bulk heterojunctions are poly (3-hexylthiophene) (P3HT)/6,6-phenyl C61-butyric acid methyl ester (PCBM) blends [7,8]. The highest efficiency of P3HT:PCBM based cells is only 4%~5% [9,10]. Further improvements are being sought to boost the efficiencies, both on the materials synthesis front as well as device engineering.

It has been estimated that among all loss pathways in modern OPV cells, optical losses account for the largest share (~38%) [11]. Thus, one key way to raise the device efficiencies is to enhance the optical absorption in the OPV active layers. Several approaches have been developed, among which the incorporation of metal nanostructures at the electrode is a promising one [12–14]. Such metallic nanostructures exhibit collective electron oscillations known as surface plasmons (SPs). Upon excitation, SPs lead to strong increase in the near-field amplitude of the incident electromagnetic (EM) field, and thus enhance the light absorption in photovoltaic layer of thin film cells. However, SP excitations only enable concentration and trapping of transverse magnetic (TM) polarized light (where E-field is in the plane normal to the metal surface), and cannot enhance the EM field for transverse electric (TE) polarized light (where E-field is parallel to the metal surface). This is not

#161810 - $15.00 USD Received 19 Jan 2012; revised 21 Mar 2012; accepted 28 Mar 2012; published 15 May 2012

desirable for a practical solar cell designs aimed at enhancing optical absorption in the active layer, because it is essential to achieve a polarization-insensitive absorption enhancement, as incoming and scattered sunlight is not preferentially polarized and includes both polarizations. In addition, some metal nanostructures such as metallic nanoparticle based schemes [15,16] do not offer conductive pathways and cannot replace ITO electrodes. On the other hand, metal nanowire grating based designs [17,18] can provide a potential alternative to ITO electrodes (the schematic is shown in Fig. 1(a)). However, such schemes either provide absorption enhancement in only one polarization [17], or provide no enhancement in either polarization [18] because a significant part of incoming light is blocked by the metal structures.

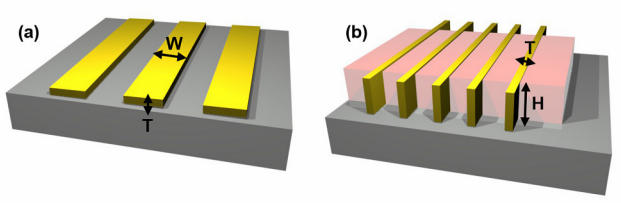

Fig. 1. (a) Conventional metal grating electrodes with nanowire/nanoribbons of width *W* and thickness *T*. Electrical conductivity increases with increasing *W*, at the cost of optical transmittance. Electrical conductivity also increases with increasing *T*, but at the cost of substrate smoothness required for solution processing conformal OPV layers. (b) Proposed metallic grating with nanowalls of thickness *T* and height *H*. Spaces between nanowalls are filled with a transparent polymeric matrix, providing a flat top surface for device fabrication (fabrication of such structures was reported in Ref. 4). Optical transmittance and electrical conductivity are largely decoupled because electrical conductivity can be increased by increasing *H*, which does not affect optical transmittance.

The architecture we proposed in Ref. 4 (Fig. 1(b)) differs from other metal grating schemes (Fig. 1(a)) in the sense that metal nanowalls are high-aspect ratio with a nanoscale footprint *T* and (sub)microscale height *H*. In other studies, either the metal ribbons are lying down flat with larger dimension facing the incoming light, or a nanowire approach is followed in which both dimensions are comparable. Compared to a conventional metal grating design shown in Fig. 1(a), there are three advantages of our design: (1) With metal ribbons very thin, the metal grating will not block the incident light. (2) Our structure provides geometric separation of electrical conductivity and optical absorption. The height of metal ribbons can be increased to increase the conductivity while minimally changing the absorption in the active layer below (we show this later). (3) Our structure gives flat top surface for device fabrication. Conventional grating design usually gives a rough surface, which can pose problems for solution processing of polymer layers because surface roughness of gratings are in the same scale as organic layer thickness, and achieving conformal polymer films becomes challenging [19]. On the other hand, in order to increase electrical conductivity for a conventional grating design, either the thickness or width (*T* and *W*, respectively, in Fig. 1(a)) of the grating needs to be increased. Increasing the thickness *T* makes the transparent electrode rougher and coating a conformal film more challenging. Increasing the width *W* will block more light. Our architecture does not suffer from this problem. The height of the grating can be increased to improve the conductivity, while still giving a flat top surface since the metallic grating is held within the polyurethane (PU) matrix.

In this report, we show that our transparent electrode architecture reported in Ref. 4 not only matches and outperforms ITO in its transparency and conductivity, respectively, but can additionally enhance light absorption in OPV active layers (we investigate the canonical P3HT:PCBM system in this report) for both polarizations. Two different mechanisms are identified to be responsible for the field enhancements for the two polarizations, respectively. For TM-polarized light, SP excitations are utilized to enhance the near EM field, while for TE-polarized light effective coupling to cavity resonance modes accounts for absorption enhancement inside the photoactive P3HT:PCBM layer. A remarkable ten folds high peak

#161810 - $15.00 USD Received 19 Jan 2012; revised 21 Mar 2012; accepted 28 Mar 2012; published 15 May 2012

light absorption enhancement at specific wavelengths and a ~23% broadband enhancement are expected using the design, when compared to an ordinary cell using a 150 nm thick ITO coated glass as the transparent electrode.

2. Simulation results and discussions

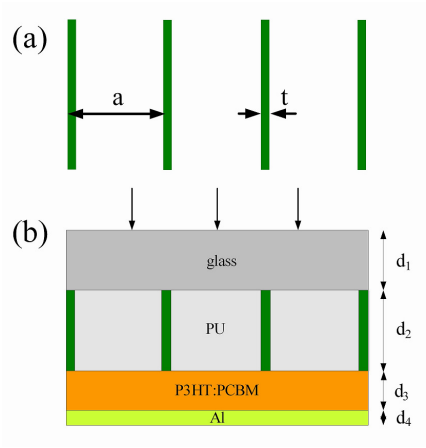

Fig. 2. (a) Top view of our 1-D metal grating with period *a* and metal thickness *t*. (b) Side view of a P3HT:PCBM based OPV cell, with the metal grating replacing ITO as the electrode.

The basic structure of the proposed design was depicted in Fig. 1(b), and is shown again in two-dimension in Fig. 2, with other device layers included, and all simulation relevant dimensions labeled. On top is a glass superstrate with a thickness of d_1. A metal grating with a height of d_2, spaced and held by a PU matrix, is sandwiched between the glass superstrate and the active P3HT:PCBM layer of thickness d_3. This metal grating acts as the top transparent electrode and replaces ITO in conventional device architecture. The grating has a feature period of *a* and the metal walls have a thickness *t*. The bottom electrode is aluminum with a thickness d_4. Unpolarized sunlight irradiates the cell from the top.

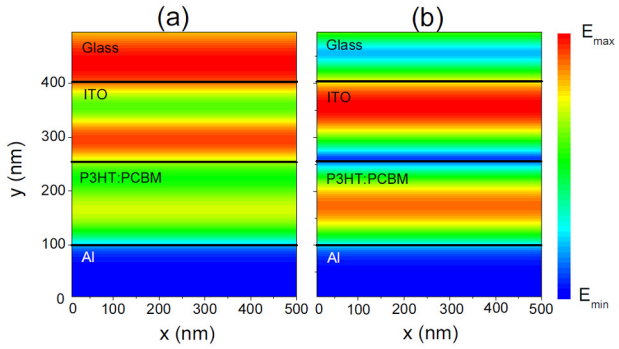

Fig. 3. Steady-state E-field intensity distribution across a common P3HT:PCBM based cell with ITO as top electrode at normal incidence. The light wavelengths are (a) 500 nm and (b) 700 nm, respectively.

To maximize the absorption in the active layer, it is important to examine the absorption's dependence on the system's geometric parameters and incident light polarizations. Plane-wave-based transfer matrix method [20–22] is applied as a full-field electromagnetic approach to obtain the absorption spectrum and the steady-state E-field distribution. In the simulation, the wavelength range is restricted to 400 to 800 nm to match the solar spectrum and P3HT:PCBM absorption. The thickness of Al electrode d_4 is fixed at 100 nm. Ag is used

#161810 - $15.00 USD Received 19 Jan 2012; revised 21 Mar 2012; accepted 28 Mar 2012; published 15 May 2012

as a metal of choice for the grating due to its promise for plasmonics [23]. Ordinary cells with ITO as top electrode are also simulated for control. Dispersive dielectric constants of Ag, Al, ITO and P3HT:PCBM with 1:1 weight ratio were obtained from Refs. 24-26.

Figure 3 shows the simulated E-field distribution across a general P3HT:PCBM based cell with ITO as top electrode. The thicknesses of ITO and the P3HT:PCBM layer are 150 nm and 160 nm, respectively. The glass superstrate is set to be infinitely thick to eliminate the interference between the light reflected from its top and bottom surfaces. At the wavelength of 500 nm (Fig. 3(a)), it can be clearly seen that the incident light intensity undergoes a decay in the P3HT:PCBM layer, which indicates absorption in the active layer. However, at the wavelength of 700 nm (Fig. 3(b)), such absorption is inconspicuous, as expected.

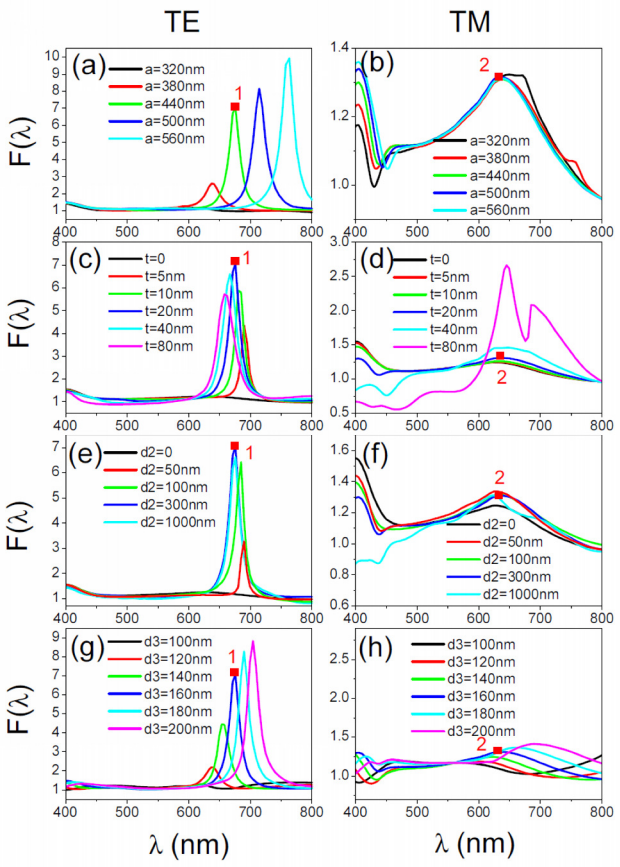

Fig. 4. Absorption enhancements versus wavelength with varying geometric parameters and polarizations. (a,b) Enhancement with varying feature period a and fixed t,d_2,d_3. (c,d) Enhancement with varying silver walls' thickness t and fixed a,d_2,d_3. (e,f) Enhancement with varying nanograting's thickness d_2 and fixed a,t,d_3. (g,h) Enhancement with varying P3HT:PCBM blends' thickness d_3 and fixed a,t,d_2. (a,c,e,g) TE incidences. (b,d,f,h) TM incidences.

Replacing ITO with our metal (Ag) grating structure may significantly enhance the absorption for long wavelength (> 600 nm). It is important to achieve so because significant amount of solar spectrum is in the red and near-infra-red region. To analyze the absorption's dependence on the system's geometric parameters, we investigated the absorption enhancement factor $F(\lambda)$, defined as the ratio of absorbed energy in the active layer for a cell with Ag grating, to that for a common cell with ITO, for a specific wavelength λ. $F(\lambda)$ is also a function dependent on the cell's geometric parameters (a,t,d_2,d_3) and polarizations of incident light. In Fig. 4(a)–4(h), we plot $F(\lambda)$ for both polarizations as a function of

#161810 - $15.00 USD Received 19 Jan 2012; revised 21 Mar 2012; accepted 28 Mar 2012; published 15 May 2012

wavelength while changing one of the system parameters (a,t,d_2,d_3) and keeping other 3 parameters fixed. The original setting is (a,t,d_2,d_3) = (440nm,20nm,300nm,160nm).

In the following paragraphs, we discuss the dependence of $F(\lambda)$ on each parameter for TE and TM polarized plane-wave illuminations. Both polarizations need to be considered for randomly polarized sunlight. For TE polarization (where E-field is parallel to the metal walls), significant absorption enhancements are present at certain long wavelengths (Fig. 4(a), 4(c), 4(e), 4(g)). In some areas, such enhancements can reach a level of ~10 times. The resonant wavelength, e.g. the peak of $F(\lambda)$, and the strength of enhancement are strongly dependent on a and d_3(Fig. 4(a), 4(g)). To obtain intense absorption enhancements, the silver walls should be thick enough and nanograting should be high enough (t≥10nm, d_2≥100nm, see Fig. 4(c), 4(e)). For TM polarization (where E-field is in the plane normal to the metal walls), absorption enhancements are generally present from short to long wavelengths in most cases (Fig. 4(b), 4(d), 4(f), 4(h)). However, for short wavelengths, adding too much silver suppresses the absorption in the active layer (see, for example, t = 80nm in Fig. 4(d) or d_2 = 1000nm in Fig. 4(f)). These enhancements are not as strong as in the case of TE incidence. The resonant wavelength is dependent on d_3 but not on a (Fig. 4(b), 4(h)), which is different from the case of TE incidence. It is worth noting that increasing d_2 from 100nm to 1000nm does not notably degrade $F(\lambda)$ for both polarizations, which is an advantage of our structure and supports our aforementioned claim that our transparent electrode architecture is able to relieve the trade-off between electrical conductivity and optical transmittance. The height of the metal nanowalls can be increased to enhance conductivity, while minimally changing the absorption in the underneath P3HT:PCBM blends.

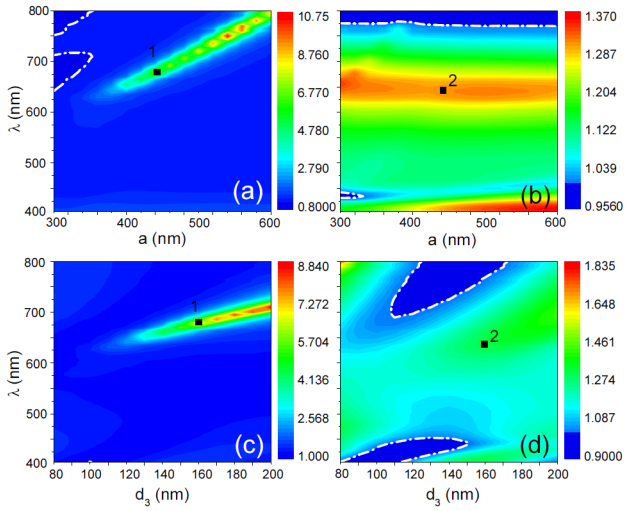

Fig. 5. Mapping the absorption enhancement with varying grating period and thickness of P3HT:PCBM. (a,b) Absorption enhancement with both wavelength and nanograting period a for TE and TM incidences, respectively. (c,d) Enhancement versus both wavelength and thickness of P3HT:PCBM d_3 for TE and TM incidences, respectively. The silver walls' thickness t and nanograting's height d_2 are 20 nm and 300 nm, respectively. The dash dot lines indicate the regions where the absorption is suppressed ($F(\lambda)$<1).

As can be seen in Fig. 4, the nanowall grating period a (for TE polarization) and P3TH:PCBM layer thickness d_3 (for both polarizations) are important parameters that decide the resonant frequency and the strength of absorption enhancement. Figure 5 further visualizes the effect of a and d_3 on absorption enhancement. A broadband polarization-insensitive absorption enhancement is observed, which is important for a practical design since incoming and scattered sunlight is not polarized and includes both TE and TM polarizations. The absorption is generally enhanced except at those locations encircled by dash dot lines. Two mechanisms can be identified and are responsible for the broad-band

#161810 - $15.00 USD Received 19 Jan 2012; revised 21 Mar 2012; accepted 28 Mar 2012; published 15 May 2012

absorption enhancement. The first mechanism is associated with cavity resonance (Fig. 5(a), 5(c)). The resonant frequency is typically dependent on the cross-sectional dimension of the cavity, i.e. the grating period a and the active layer thickness d_3. The resonant wavelength shifts to red with increasing a and/or d_3. The second mechanism is due to SP resonance, which can be excited only with TM polarization (Fig. 5(b), 5(d)). The resonant frequency is much less affected by the period a, and shifts to red with increasing d_3.

To further investigate the two absorption enhancement mechanisms, we plot in Fig. 6 the electric field distribution at the resonant frequencies for the cavity resonance and SP resonance modes, respectively. Figure 6(a) shows TE electric field distribution corresponding to point 1 in Fig. 4(a), 4(c), 4(e), 4(g) and Fig. 5(a), 5(c), at wavelength of 670 nm, with system parameters (a,t,d_2,d_3) = (440nm,20nm,300nm,160nm). The characteristic of a highly localized cavity resonant mode with a standing wave pattern can be clearly seen. The resonant frequency is decided by the dimension of the cavity (a,d_3), as illustrated in Fig. 5(a), 5(c). By comparing with the field profile in an ordinary cell with 150 nm thick ITO shown in Fig. 6(b), a remarkable field enhancement is observed, indicating a strong absorption enhancement, as the absorption is proportional to the square of E-field intensity. A TE enhancement is also achieved in a recent work by Guo and associates [23], but the enhancement is weaker than ours. The TE field in Guo's nanowire grating design is not as well localized as in our nanowall gratings. It is also worth noting that this cavity resonant mode is more robust than the SP resonant mode as shown in Fig. 6(c) for TM polarization (corresponding to point 2 at wavelength of 630 nm in Fig. 4(b), 4(d), 4(f), 4(h) and Fig. 5(b), 5(d)), since SP excitations are sensitive to the metal roughness. These SP excitations enhance the field at the surface of P3HT:PCBM blends just under the Ag grating. Moreover, they couple to an antenna-like mode, resulting in an field enhancement deeper inside the P3HT:PCBM blends.

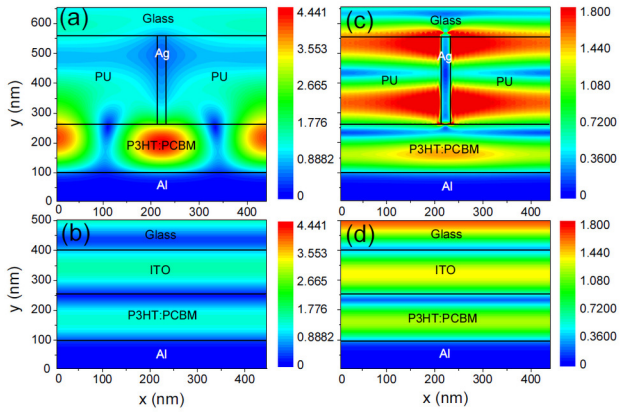

Fig. 6. Time-averaged electric field distribution across the cell structure at normal incidence. (a,c) A cell with Ag grating is illuminated at wavelengths of 670 nm at TE and 630 nm at TM polarizations, respectively. (b,d) A normal cell with 150 nm thick ITO is illuminated at wavelengths of 670 nm and 630 nm as a reference. The Ag nanograting has a = 440nm, t = 20nm, d_2 = 300nm, and the P3HT:PCBM blends has d_3 = 160nm.

To obtain a full evaluation on the design, we need to consider the total enhancement in the short circuit current that can be expected from the presence of the metal nanograting. It is assumed that a cell's short circuit current is proportional to the number of photons being absorbed. Let $I(\lambda)$ be the distribution of photon number on the wavelength, based on the standard AM1.5 (air mass) spectrum. The total absorption enhancement (also enhancement in the short circuit current) can be expressed as

#161810 - $15.00 USD Received 19 Jan 2012; revised 21 Mar 2012; accepted 28 Mar 2012; published 15 May 2012

$$F_{tot} = \frac{\frac{1}{2}\left(\int I(\lambda)F_{TE}(\lambda)d\lambda + \int I(\lambda)F_{TM}(\lambda)d\lambda\right)}{\int I(\lambda)d\lambda}, \quad (1)$$

taking into account equal contribution of incident TE and TM polarized light. In the integration, λ varies from 400 nm to 700 nm given the band-gap of P3HT is 1.8 eV. The calculated short circuit current enhancement is ~19%, with the same system parameters as before (a,t,d_2,d_3) = (440nm,20nm,300nm,160nm).

Finally, we consider the absorption enhancement in the presence of a thin poly(3,4-ethylenedioxythiophene):poly(styrenesulfonate) (PEDOT:PSS) layer sandwiched between the top electrode (Ag nanograting or ITO) and P3HT:PCBM blends. In a real device, a layer of PEDOT:PSS is typically used to smooth the ITO surface, decrease the density of pinholes and increase the work function to enhance hole collection [27]. It will also be crucial to use PEDOT:PSS in our metal-grating based transparent electrodes, in order to collect and transport holes in regions between two adjacent metal walls. High conductivity PEDOT:PSS formulations can efficiently do hole transport even over distances greater than 100 micrometers [28]; in our design the distance between two metallic nanowalls is only more or less than just a micron. We did not include this PEDOT:PSS layer in previous calculations since it is thin compared to other layers. In Fig. 7, we plot the enhancement factor $F(\lambda)$ in the presence of a 30 nm thick PEDOT:PSS film for both TE and TM illuminations. As a reference, $F(\lambda)$ without PEDOT:PSS is also plotted. The resonant frequency shows a slight shift to red in the presence of the PEDOT:PSS film, while the level of enhancements almost remain the same. The system parameters are the same as before (a,t,d_2,d_3) = (440nm,20nm,300nm,160nm). The total absorption enhancement can be calculated to be ~23% using Eq. (1). The use of a high conductivity PEDOT:PSS film (not shown) results in a nearly identical plot of $F(\lambda)$. The dispersive refractive indices and extinction coefficients of ordinary and high conductivity PEDOT:PSS with sorbitol were obtained from Ref. 29.

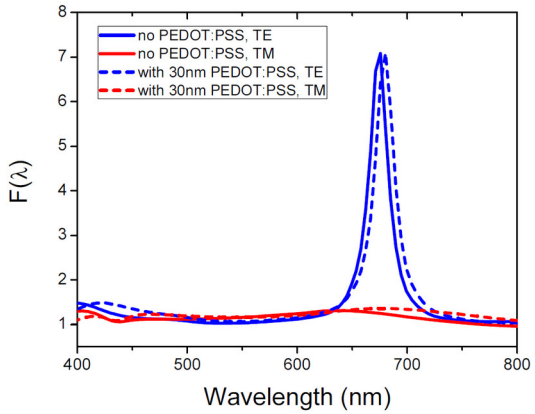

Fig. 7. The absorption enhancement factor with/without a 30 nm thick PEDOT:PSS layer for both TE and TM polarizations. The system parameters are a = 440nm, t = 20nm, d_2 = 300nm, d_3 = 160nm.

3. Summary

In conclusion, a unique thin film solar cell design is proposed, which includes an embedded metal nanowall grating as the transparent electrode. The design is studied for P3HT:PCBM solar cells in regards to effect on optical absorption within the photovoltaic layer. Both broadband and polarization-insensitive absorption enhancement can be realized with the metal nanowall grating. Two mechanisms, the cavity resonance and SPs resonance are identified to be responsible for the enhancement. In summary, our high aspect-ratio metal

#161810 - $15.00 USD Received 19 Jan 2012; revised 21 Mar 2012; accepted 28 Mar 2012; published 15 May 2012

nanowall grating (with only nanoscale footprint that blocks light, and (sub)microscale height that enable high electrical conductivity) is able to achieve both goals: (i) replace ITO electrode, and (ii) achieve a broadband and polarization-insensitive absorption enhancement.

Acknowledgments

This work is supported by the Division of Materials Sciences and Engineering, Basic Energy Sciences, US Department of Energy. The Ames Laboratory is operated by Iowa State University for the Office of Science, U.S. Department of Energy under Contract DE-AC02-07CH11358. SC acknowledges support by National Science Foundation (ECCS – 1055930) for financial support.

#161810 - $15.00 USD Received 19 Jan 2012; revised 21 Mar 2012; accepted 28 Mar 2012; published 15 May 2012